Determination of math xmlns="http://www.w3.org/1998/Math/MathML">mi>β/mi> /math>-decay feeding patterns of math xmlns="http://www.w3.org/1998/Math/MathML">mmultiscripts>mi>Rb/mi>mprescripts>/mprescripts>none>/none> mn>88/mn>/mmultiscripts>/math> and math xmlns="http://www.w3.org/1998/Math/MathML">mmultiscripts>mi>Kr/mi>mprescripts>/mprescripts>none>/none>mn>88/mn>/mmultiscripts>/math> using the Modular Total Absorption Spectrometer at ORNL HRIBF

P. Shuai et al.

Phys. Rev. C **105**, 054312 — Published 18 May 2022

DOI: 10.1103/PhysRevC.105.054312

Determination of β-Decay Feeding Patterns of ^{88}Rb and ^{88}Kr Using The Modular Total Absorption Spectrometer

P. Shuai,[1,2,3,4] B. C. Rasco,[1,2,3,*] K. P. Rykaczewski,[2] A. Fijałkowska,[5,3] M. Karny,[5,2,1] M. Wolińska-Cichocka,[6,2,1] R. K. Grzywacz,[3,2,1] C. J. Gross,[2] D. W. Stracener,[2] E. F. Zganjar,[7] J. C. Batchelder,[8,1] J. C. Blackmon,[7] N. T. Brewer,[1,2,3] S. Go,[3] M. Cooper,[3] K. C. Goetz,[9,3] J. W. Johnson,[2] C. U. Jost,[2] T. T. King,[2] J. T. Matta,[2] J. H. Hamilton,[10] A. Laminack,[2] K. Miernik,[5] M. Madurga,[3] D. Miller,[3,11] C. D. Nesaraja,[2] S. Padgett,[3] S. V. Paulauskas,[3] M. M. Rajabali,[12] T. Ruland,[7] M. Stepaniuk,[5] E. H. Wang,[10] and J. A. Winger[13]

[1]*JINPA, Oak Ridge National Laboratory, Oak Ridge, Tennessee 37831, USA*
[2]*Physics Division, Oak Ridge National Laboratory, Oak Ridge, TN 37831, USA*
[3]*Dept. of Physics and Astronomy, University of Tennessee, Knoxville, TN 37966, USA*
[4]*Institute of Modern Physics, Chinese Academy of Sciences, Lanzhou, Gansu 730000, China*
[5]*Faculty of Physics, University of Warsaw, Pasteura 5, PL-02-093 Warszawa, Poland*
[6]*Heavy Ion Laboratory, University of Warsaw, PL-02-093 Warszawa, Poland*
[7]*Dept. of Physics and Astronomy, Louisiana State University, Baton Rouge, LA 70803 USA*
[8]*Department of Nuclear Engineering, University of California, Berkeley, Berkeley California 94720, USA*
[9]*CIRE Bredesen Center, University of Tennessee, Knoxville, TN 37966, USA*
[10]*Dept. of Physics and Astronomy, Vanderbilt University, Nashville, TN 37212, USA*
[11]*Chemical and Radiation Measurements Department, Idaho National Laboratory, Idaho Falls, ID 83415, USA*
[12]*Department of Physics, Tennessee Technological University, Cookeville, Tennessee 38505, USA*
[13]*Department of Physics and Astronomy, Mississippi State University, Mississippi State, Mississippi 39762, USA*

(Dated: April 22, 2022)

Precise determination of ground-state feeding in the β decay of fission products is an important but challenging component in modeling reactor anti-neutrino flux and reactor decay heat. The Modular Total Absorption Spectrometer (MTAS) is a versatile NaI(Tl) detector array that determines the true β-decay pattern free from the Pandemonium Effect, including precise ground-state feeding intensities. In this paper, we report MTAS results of the β feeding intensities of ^{88}Rb and ^{88}Kr, fission products with large cumulative yields in nuclear reactors. By comparing MTAS results with previous measurements, ^{88}Rb provides an validation of MTAS ability to determine ground-state feedings in β decays, while the precision of ^{88}Kr ground-state feeding is improved when compared with the Evaluated Nuclear Structure Data File (ENSDF). The investigation of sources that contribute to β feeding branching uncertainties in MTAS experiments is discussed in details. Lastly, the deconvolution of ^{88}Rb decay spectra suggests that MTAS can distinguish an allowed β spectral shape from a first forbidden unique β spectral shape.

I. Introduction

Total Absorption Spectroscopy (TAS) is an important β decay measurement technique. It was originally envisioned to overcome the difficulties in accurately measuring β-decay feeding patterns of complex β decays, often referred to as the Pandemonium Effect [1]. Since the initial experiments [2, 3] TAS has demonstrated abilities to overcome multiple experimental challenges posed by early, low-efficiency detection systems. These include direct measurement of ground-state to ground-state β feedings (hereafter referred to as ground-state feeding) and challenges with insufficient data required to establish multiple-γ coincidence relationships. These challenges lead to potentially incomplete β-feeding patterns, I_β, in the current nuclear data [4]. The need to revise potential incomplete older measurements was articulated in many recent TAS publications [5–9].

Incomplete nuclear β-decay data negatively impacts many basic research and applications. A partial list includes nuclear reactor decay heat [7], measurements and evaluations of $\bar{\nu}_e$ spectra emitted from reactors [10–14], nuclear reactor safety and design, reactor monitoring, as well as the elemental abundances in the galaxy and exotic physics searches [15]. These diverse research areas depend on accurate and precise nuclear data; hence it is essential to measure β decays with multiple experimental approaches. Two complimentary methods for β-delayed γ-ray spectroscopy measurements are high energy resolution, low-efficiency measurements with the High Purity Germanium (HPGe) arrays, and the TAS technique. TAS detectors are based on inorganic scintillators such as NaI with very high efficiency but reduced energy resolution. Due to the limitations of each method, it is desired to employ both experimental techniques when feasible to obtain the most reliable nuclear data. The strength of TAS is its ability to address the Pandemonium Effect [1]. The Pandemonium Effect, in brief, arises from the many weak β feedings of close-spaced levels at high excitation energies, followed by the cascades of weak γ transitions. As recently demonstrated [5, 6, 16], TAS is also an excellent method to measure the ground-state feeding.

The TAS measurements typically lead to a revision of the nuclear data obtained using high-resolution spectroscopy. First, addressing the Pandemonium Effect, feeding to a highly excited nuclear state increases, equivalently increasing the average γ energy and decreasing the average leptonic (β and $\bar{\nu}_e$) energy. Second, measuring the ground-state feeding may either increase or decrease the emitted average γ energy in

current nuclear data, depending on whether the ground-state feeding is overestimated or underestimated. Often ground-state feedings have not been directly measured at all. Uncertainty in the ground-state feeding have a particularly large impact on reactor $\bar{\nu}_e$ emission spectra, since this is the only decay branch where the $\bar{\nu}_e$ can carry away the full β decay energy. This is where many high energy (5 - 9 MeV) reactor $\bar{\nu}_e$ may originate. Due to a lack of associated γ-rays for ground-state feedings, measurements of ground-state feedings in β decay are challenging and suffer from large uncertainties [5], even for some nuclei near β stability. The nearby examples of imprecisely measured ground-state feeding intensities I_β (gs-gs) include ^{88}Br and ^{88}Se. ^{88}Br has an ENSDF-assessed I_β (gs-gs) of < 11% based on upper limit calculated from the sum of the I_β intensities [17]. While ^{88}Se has been measured indirectly twice, yielding I_β (gs-gs) values of 20.5% and 38%, the logft estimations points to an expected ground-state feeding of < 3% [17–19]. Determination of the ground-state feeding of reactor-abundant fission products with increased precision is required to improve decay heat analysis as well as the properties of the $\bar{\nu}_e$ flux. Due to these types of incompleteness affecting β-decay measurements it is important to either validate or correct the current nuclear data.

There have been several reports assessing important β decays that affect decay heat and reactor $\bar{\nu}_e$ fluxes [20–22]. An IAEA report about the assessment of decay heat calculation from irradiated Th/U fuel gives a recommended list of important isotopes that are required to be measured by total absorption spectroscopy experiments [21]. In this report, ^{88}Rb is estimated to contribute about 5% total decay heat after a cooling time of 5000 s and 8.9% after a cooling time of 10000 s for the thermal-neutron irradiated Th/U fuel. Because of this large contribution at late cooling times, ^{88}Rb is recommended with high priority to be measured using TAS for accurate decay heat analysis.

Many important fission products have been measured with the Modular Total Absorption Spectrometer (MTAS) [5, 6, 23] profiting from unprecedented MTAS efficiency and modularity allowing to directly establish the β-feeding patterns. In this paper the total absorption spectra measured with the MTAS detector for the β-feeding intensities of ^{88}Rb and ^{88}Kr are reported and analyzed. It is also demonstrated that MTAS can distinguish a first-forbidden-unique β shape compared with an allowed β shape for the ^{88}Rb ground-state feeding. The current ^{88}Rb and ^{88}Kr ground-state feeding intensities are validated, while improving the ^{88}Kr precision, providing confirmation of MTAS's ability to determine the ground-state feeding. Additionally a detailed discussion of uncertainty evaluation in MTAS data analysis is presented.

II. Experiment and Data Analysis

The experiments were performed at the Holifield Radioactive Ion Beam Facility (HRIBF) at the Oak Ridge National Laboratory [24]. A 40-MeV proton beam irradiated a ^{238}UCx target that was close-coupled to an ion source [25]. Fission products were extracted from the ion source, selected by a mass separator [24], and then implanted onto a tape that transported the radioactive samples into MTAS [26]. A complete measurement cycle includes several steps: implantation, pause for short-lived nuclei to decay away, transport the samples into the center of MTAS, measurement and move the samples away to a shielded chamber. The time setting for each step is determined by considering the impact of half-lives of the nuclei of interest and possible contamination on the quality of experimental data.

Two different ion sources were applied to deliver ^{88}Kr and ^{88}Rb beam. For the ^{88}Kr [$T_{1/2} = 2.825(19)$h, $Q_\beta = 2.918(3)$MeV] measurement, a LaB_6 source that produces negative ions delivers ^{88}Br beam. Ions were collected for 30 min. After the tape pausing for 160 sec to allow the ^{88}Br ions [$T_{1/2} = 16.34(8)s$] to decay away, the remaining ions on the tape were transported into MTAS and measured for 400 minutes. Only one long cycle was used for the ^{88}Kr measurement. Since ^{88}Br is a neutron emitter, $P_n = 6.58(18)\%$ [27], the ^{88}Kr spectra contain a small fraction of ^{87}Kr contamination. For the ^{88}Rb [$T_{1/2} = 17.773(11)$min, $Q_\beta = 5.3124(11)$MeV] measurement, a tantalum surface ionization source that produces positive ions delivered ^{88}Rb beam. Ions were collected for 3 min, then the sample ions were transported into MTAS and measured for 10 minutes. 5 cycles were repeated to accumulate statistics. Signals from MTAS and auxiliary detectors were recorded using Pixie16 modules, Rev.D, XIA LLC [28]. Two segmented silicon detectors in the center of the MTAS provided high efficiency β trigger signals to suppress background events [26]. MTAS consists of 19 NaI(Tl) modules that are arranged in a honeycomb structure. Based on the distance to the central axis of MTAS, these modules are sorted as the Center module, the Inner (I) ring, the Middle (M) ring and the Outer (O) ring. The sum of all the energy deposits in each module from a decay event is the total MTAS energy.

A Bayesian-based iterative technique [29, 30] is applied to deconvolve MTAS spectra. In the deconvolution algorithm, simulated response functions of each decay path are required, where a decay path is defined as the β decay of parent nuclei populated to an excited state of decay daughter and followed by one possible γ cascade to the final ground state of the daughter nuclei. The MTAS response functions for each decay path involving γ and β radiation were produced using Monte Carlo simulation code developed based on GEANT4 toolkit (version 10.5.1). We have also tested several patches of GEANT4 10.6 and 10.7, the differences of MTAS responses using different GEANT4 version are minimal. The MTAS response functions have been validated using calibration sources [26, 31] and simpler decay schemes[6, 32, 33].

Fitting only the total MTAS spectrum is not sufficient to determine details of the γ cascades, which leads to large uncertainty for the feeding intensities to higher excited states due to the variance of MTAS detection efficiency for multiple γ rays. Coincidence spectra between the total MTAS and individual modules are important supplementary information

that constrain the multiplicity and γ energies [6, 23, 32]. We extend this deconvolution algorithm to accommodate coincidence spectra so that many different MTAS spectra can be fitted simultaneously. A detailed description is provided in Appendix A.

III. Results and Discussions

A. ^{88}Rb decay

The ^{88}Rb beam was very pure due to extraction of positive ions from a tantalum surface ionization source. ^{88}Br ions are negative and ^{88}Kr is noble gas, therefore these two species were not extracted from this ion source. The half-life obtained from the time vs. the total MTAS spectra is 17.9(2) min, in agreement with the ENSDF value 17.773(11) min. The major peaks from ^{87}Kr and ^{88}Kr decays are not observed in MTAS spectra of ^{88}Rb. Therefore, the contamination from these two nuclei is minimal and the associated impact on the uncertainty of ^{88}Rb feeding intensity is discussed in the next subsection. In Fig. 1 the deconvolution results of background subtracted MTAS spectra of ^{88}Rb are shown. The scaled response functions of each decay path with feeding intensity larger than 0.1% are also plotted. No new levels are required to reproduce the total MTAS spectra.

Besides the total MTAS spectra, two coincidence spectra are deconvolved simultaneously, including the Center module vs. the total MTAS, and the individual modules in I. M. O. rings vs. the total MTAS, see [23]. The response function of each decay path of ^{88}Rb is simulated using GEANT4 toolkit. These are used to create the response function matrix. The MTAS spectra of ^{88}Rb are used as input to the deconvolution algorithm described in Appendix A. From the results of this deconvolution the feeding intensity of each decay path is obtained. These results are listed in Table IV in Appendix. C. By adding the feeding intensities fed to the same level in Table IV, the feeding intensities for each level are calculated. These along with the results from previous experiments are listed in Table I. The uncertainty of the β feeding intensity of each level listed in Table I is the total uncertainty which takes into account all the possible sources discussed in Sec. D. The intensity of the dominant ground-state feeding is determined to be 78.2(20)%. The comparison of the total MTAS spectra to the simulated spectra using ENSDF data with first-forbidden-unique ground-state transition $2^- \rightarrow 0^+$ [34] does not reveal a visible differences. Our results are more consistent with the results from [34, 35], but agree with the recommended values from ENSDF within 1σ uncertainty. The data from [36] contributes the highest weight among all the relevant references adopted in ENSDF, but their systematic uncertainties may be underestimated.

TABLE I. β intensities of ^{88}Rb determined by MTAS in comparison with ENSDF data and previous results.

Level (keV)	ENSDF (%)	Ref. [36]	Ref. [34]	Ref. [37]	Present work
0	76.51(11)	76.58(25)	77.4(14)[35]	76.2(40)	78.2 (20)
1836	4.93(24)	4.59(20)	4.3(4)	4.7	4.22(39)
2734	13.59(21)	13.89(14)	13.7(9)	13.8	12.8(12)
3218	1.038(12)	1.043(11)	1.01(7)	1.1	1.06(10)
3486	0.016(11)	0.017(17)	0.018(15)	0.14	0.020(2)
3524	<0.003	0.0053(10)	0.007(4)		0.03^{+9}_{-3}
3634	0.005(6)	0.0055(59)	∼0	0.12	0.04^{+11}_{-4}
4035	0.0137(21)	0.013(2)	0.011(2)		0.014^{+36}_{-14}
4224	0.030(3)	0.030(3)	0.029(9)		0.008^{+57}_{-8}
4413	0.254(9)	0.232(7)	0.216(19)	0.16	0.47(25)
4514	2.319(22)	2.31(2)	2.18(14)	3.0	1.87(30)
4742	0.178(19)	0.183(15)	0.147(11)	0.14	0.22(10)
4845	0.401(6)	0.391(6)	0.37(3)	0.23	0.59(5)
4853	0.726(13)	0.711(18)	0.68(5)	0.56	0.46(10)

B. The character of ground state β-transition in ^{88}Rb decay

The ground-state feeding of ^{88}Rb β decay is a first forbidden unique transition $2^- \rightarrow 0^+$ [34]. We use two β-shape functions to generate the ground-state response function. For an allowed transition, the shape factor $C(W) = 1$, where W is the total energy of the electron. For a first forbidden unique transition, the shape factor used in the simulation is $C(W) = p^2 + q^2$, where p is the normalized momentum of electron and q is the neutrino momentum [38]. Fig. 2(a) shows the input β kinetic energy distribution of the ground-state feeding of ^{88}Rb, assuming an allowed transition and a first forbidden unique transition. The corresponding MTAS response functions are shown in Fig. 2(b). The maximum energy detected in both β response functions are shifted down by $\sim$ 1.2 MeV from Q_β due to the energy loss of electrons in the dead layers before entering MTAS. The difference of two β kinetic energy distribution below 3 MeV is washed out in the MTAS response functions due to bremsstrahlung radiation. The dominant difference of the two response functions is between 2 - 4 MeV, which comes from β electrons with kinetic energy larger than $\sim$ 3.2 MeV.

Fig. 3 shows the deconvolution results of the Center-module-only spectra using the two different shape functions of ground-state feeding described above. The Center-module-only spectra require no energy deposit in any other module, most of MTAS is an active veto. The importance of this spectra is that the response of β feeding to higher excited states is suppressed, and the contribution of ground-state feeding is enhanced. Defining the reduced fitting χ^2 over the range of 2 - 4 MeV as

$$\chi^2 = \sum_{i=2000}^{4000} \frac{(N_i - N_i^{fit})^2}{N_i(2000 - DOF)}, \quad (1)$$

where N_i is the counts in the i-th bin and $DOF = 54$ is the

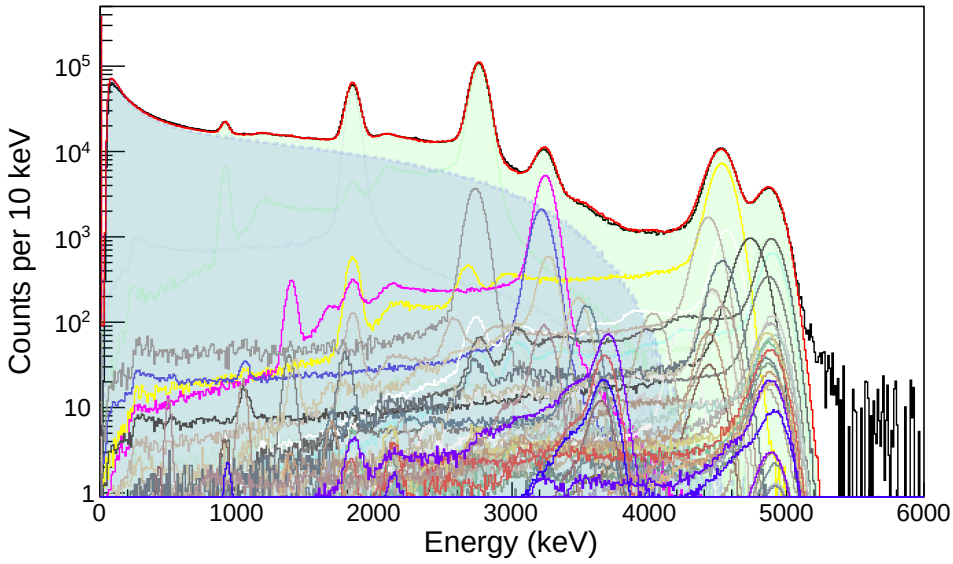

FIG. 1. Deconvolution of background subtracted MTAS spectra of ^{88}Rb (Black line). The red curve with green shadow, which is the sum of all the fitted response functions (rainbow palette), reproduces the MTAS spectra very well. The dash line with blue shadow is the response function of ground-state feeding. The bremsstrahlung peak is the large increase below 500 keV from ground-state feeding.

total number of decay paths, the deconvolution quality with two different shape functions can be compared. The reduced χ^2 with a first forbidden unique shape is 3.6, while the number is 6.5 using an allowed shape. The reduced χ^2 decreases by almost a factor of 2, suggesting MTAS can distinguish an allowed β shape from a first forbidden unique β shape.

C. ^{88}Kr decay

^{88}Kr and ^{88}Rb are in equilibrium, about 41% ions on the tape were ^{88}Kr after 30 min implantation. Since the ^{88}Rb spectra was also measured, we use the experimental spectrum to normalize the ^{88}Rb component. There is no clean peak from ^{88}Rb decay that can be used to normalize the ^{88}Rb component, so the subtraction of ^{88}Rb provides additional uncertainty to the feeding intensities of ^{88}Kr. This also leads to challenges to precisely determine the half-life of ^{88}Kr.

Several methods have been used to properly estimate the source components of ^{88}Rb decay. The best solution is to minimize the normalization uncertainty by including the cycle time vs. total MTAS spectra in the deconvolution. The merits of this method are (1) no statistics are lost and (2) all the information in MTAS spectra are included to constrain the normalization uncertainty. Other methods that have larger normalization uncertainty are briefly described below. Gating on early and late time does not work due to the ^{88}Kr-^{88}Rb equilibrium. Normalizing on peaks is challenging due to a lack of cleanly identified peaks. The spectrum at 4-5 MeV which is beyond the Q_β of ^{88}Kr were used to normalize ^{88}Rb, but the

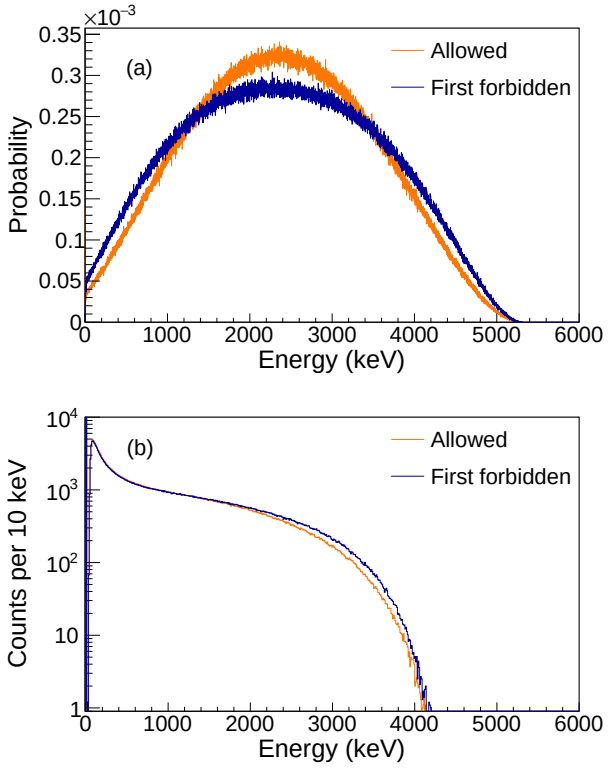

FIG. 2. Panel (a) presents the theoretical calculation of the β kinetic energy distribution in ground-state feeding of ^{88}Rb, assuming an allowed transition (orange) or a first forbidden unique transition (blue). Panel (b) displays the corresponding total MTAS response functions.

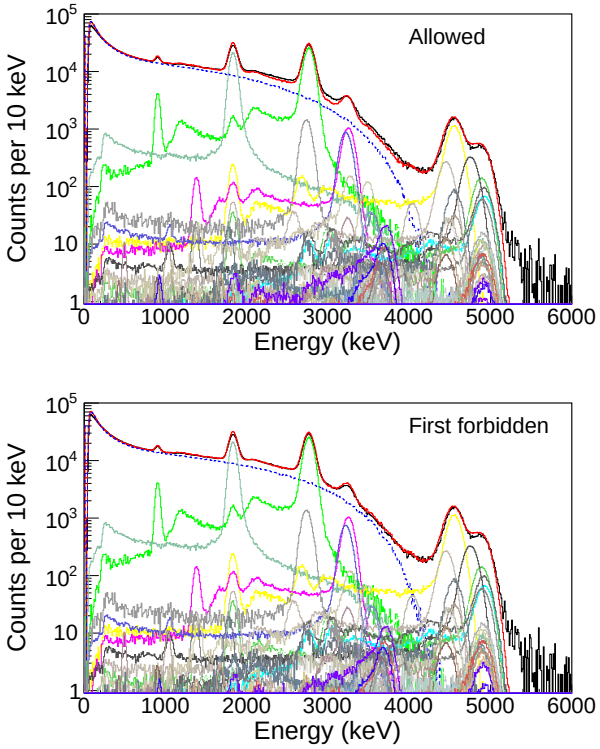

FIG. 3. Fit of the simulated response functions to the Center-module-only spectra. The I, M, O modules are used as an active veto. In the first figure, the response function of ground-state feeding is simulated as an allowed transition. In the second figure, the response function of ground-state feeding is simulated as a first forbidden unique transition.

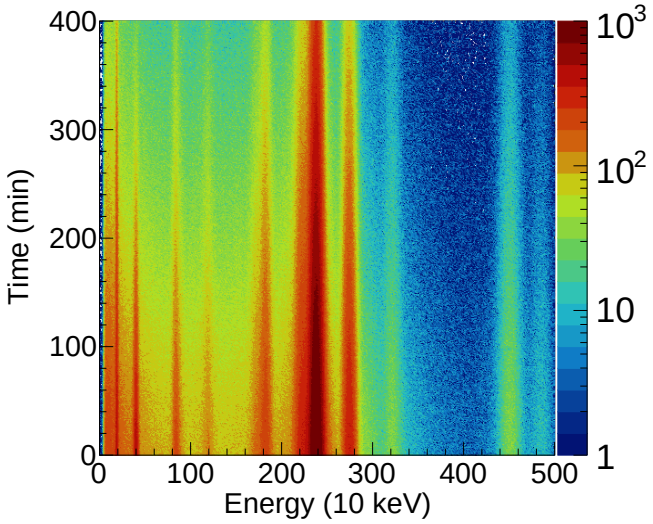

FIG. 4. Two dimensional spectra of cycle time vs. total MTAS energy. The sum of energy deposit in all MTAS modules is plotted in X-axis, while the cycle time is plotted in Y-axis.

β-feeding to levels above 4 MeV in ^{88}Rb is small, leading to a normalization factor that is largely affected by background coincidence events.

Fig. 4 illustrates the time vs. total MTAS spectra of ^{88}Kr. There are 3 different components in the spectra: ^{88}Kr decay, ^{88}Rb decay, and small fraction of ^{87}Kr decay that comes from the βn branch of ^{88}Br. The ^{88}Kr and ^{87}Kr follow simple exponential decay, because the tape pause after implantation removes all parent activities. The ^{88}Rb decay contains both the parent-independent decays from the initial collection of ^{88}Rb during implantation and the parent-related decays from the decay daughter of ^{88}Kr. Only the total decays of ^{88}Rb from the parent-related decays should be equal to the total decays of ^{88}Kr. Since the half-life of the nuclei involved are well measured, the response function of the total MTAS energy for each decay path is used to generate the corresponding response function of time vs. total MTAS. Details of this method are described in Appendix. B.

By fitting the cycle time vs. total MTAS energy spectra along with the total MTAS spectra and individual module vs. total MTAS spectra, the normalization uncertainty of ^{88}Rb is reduced. The fitted time vs. total MTAS spectra for each components are illustrated in Fig. 5, the sum of these four spectra reproduces the time vs. total energy MTAS spectra in Fig. 4. The deconvolution results of total MTAS energy spectra are shown in Fig. 6. The overall uncertainty of ground-state feeding is reduced, with MTAS-derived ground-state β-feeding of $12.9(25)\%$ after including the time vs. total MTAS spectra in the fit, an improved value in comparison to $14(4)\%$ in ENSDF [35]. The ground-state feeding of ^{88}Kr reported here includes the direct β-feeding to the 27 keV level, since their MTAS response functions are indistinguishable. But the spin-parity of the 27 keV level is tentatively assigned as (3^-), which means this transition is a third forbidden non-unique transition, therefore the direct β-feeding to this level should be very small.

The ground-state feeding of ^{88}Kr decay is also a first forbidden unique transition $0^+ \rightarrow 2^-$. We tested the impact of theoretical β shape to the ground-state feeding as we did for ^{88}Rb. The comparison of β-energy distribution of ground-state feeding assumes an allowed transition or a first forbidden unique transition, similar as FIG. 2(a), except the end point is 2.9 MeV for the ^{88}Kr decay and there is a slight change to the Fermi function due to a different Z value. The comparison of the response functions is similar to FIG. 2(b), with a lower Q_β and the largest differences between 0.5 - 2 MeV. In principle, MTAS can distinguish the allowed β-transition from first forbidden unique one for the ground-state feeding of ^{88}Kr. However, as shown in Fig.6, the ground-state feeding of ^{88}Kr at higher energies is swamped by ^{88}Rb decays. Therefore it is not possible to see the difference between an allowed shape and first forbidden unique shape in the decovolution. The impact of this on the ground-state feeding intensities is small and it is discussed in the next section.

To be more general, this method to distinguish allowed and

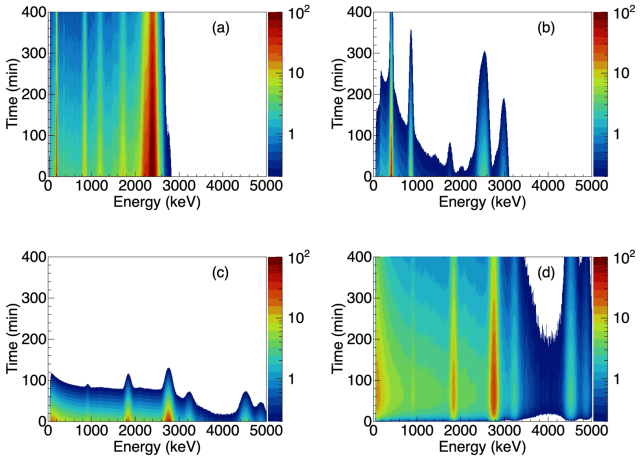

FIG. 5. Four components involved in the time-dependent ^{88}Kr spectra. (a) is the sum of all the response functions of each decay path in ^{88}Kr decay, weighted by the fitted scale factor. These response functions of each decay path in ^{88}Kr decay are generated using GEANT4 simulation and Bateman equation. (b), (c) and (d) are the ^{87}Kr spectra, parent-independent ^{88}Rb spectra and parent-related ^{88}Rb spectra respectively and normalized with the fitted scale factor. The superposition of these four plots can reproduce the cycle time vs. total MTAS energy spectra of ^{88}Kr (Fig. 4). From (a) and (d), the total number of decays from precursor and decay daughter are deduced respectively.

TABLE II. β intensities of ^{88}Kr determined by MTAS in comparison with ENSDF data and previous results.

Level (keV)	ENSDF (%)	Ref. [34]	Present work
0	14(4)	13(5)	12.9(25)
27	~ 0	~ 0	
196	2.0(3)	1.8(3)	1.7(2)
268	~ 0	~ 0	0.008(8)
362	~ 0	~ 0	0.007(7)
391	0.26(10)	0.23(9)	0.007(7)
862	1.3(3)	1.3(3)	1.3(2)
1141	0.10(6)	0.11(5)	0.17(8)
1182	1.02(7)	1.03(7)	0.78(9)
1213	~ 0	~ 0	0.17(5)
1245	~ 0	~ 0	0.14(5)
1352	~ 0	~ 0	0.04(2)
1442	0.22(3)	0.23(3)	0.02(2)
1604	~ 0	~ 0	0.01^{+2}_{-1}
1661	0.23(4)	0.23(4)	0.22(4)
1715	1.92(12)	1.94(13)	1.51(18)
1793	0.035(14)	0.035(14)	0.026(2)
1916	0.204(17)	0.207(20)	~ 0
2089	0.14(3)	0.14(3)	~ 0
2232	9.1(5)	9.1(6)	8.3(2)
2392	67(4)	67.5(40)	67.3(25)
2456	0.066(17)	0.066(18)	0.20(10)
2548	2.65(16)	2.68(19)	3.2(3)
2771	0.353(25)	0.36(3)	<1.8

first forbidden unique transitions for ground-state feeding requires a Q_β larger than approximately 2.5 MeV. This minimum Q_β is needed in order to distinguish β particles that deposit energy directly in MTAS and do not overlap with the Bremsstrahlung peak that is dominant below 0.5 MeV in the response function. A second requirement is a wide region at the decay scheme, where there are few to no excited β-populated states in the daughter nucleus, that overlaps with the largest difference between the allowed and first-forbidden unique ground-state response functions. The applicability of this new method for specific nuclei needs to be checked case by case.

D. Uncertainty Evaluation

The uncertainty of β-feeding intensities determined by MTAS measurements is affected by many sources. The analysis relies on GEANT4 simulations, and some of the uncertainty sources are correlated, so it is challenging to give an analytic expression to define an overall uncertainty [40]. In previous total absorption spectroscopy measurements, the uncertainty evaluation was handled conservatively. Here, we demonstrate the impact of individual sources that contribute to the error budget. We do this by varying one specific variable while keeping the other variables constant. In this way, we separate the contribution from different sources to the uncertainty of β-feedings, and get an idea of the magnitude of the associated uncertainties. Then we combine all these uncertainties into the final errors.

1. GEANT4 simulation of MTAS response functions.

The simulation of the MTAS response function is based on individual decay paths as defined in Sec. II. The simulation of the nonlinear light output of NaI(Tl) in MTAS is presented in [31]. The calibration of the MTAS γ efficiency using ^{137}Cs and ^{65}Zn source is shown in [26, 33]. The GEANT4 simulation well reproduces the γ spectrum and detection efficiency from source calibrations.

The largest uncertainty comes from the simulation of β particles, which impacts the ground-state feeding. There are two major challenges to simulate the ground state response. One is to precisely simulate the geometric structure in the center of MTAS, the other is the theoretical β spectrum. The simulated bremsstrahlung peak as described in Fig. 1 is very sensitive to the modeled interior structure in MTAS, including the precise arrangement of Si detector cables and the Center module housing, but it is relatively insensitive to the input of β energy spectrum. The high energy β particles are less sensitive to the MTAS interior structure and more sensitive to the input β energy spectrum.

There are two key factors to validate the simulated response function of ground-state feeding, the spectral shape and the average MTAS β efficiency. The average MTAS β efficiency is defined as the number of simulated events that deposit non-zero energy in MTAS over the total number of the simulated events for the ground-state feeding. We have com-

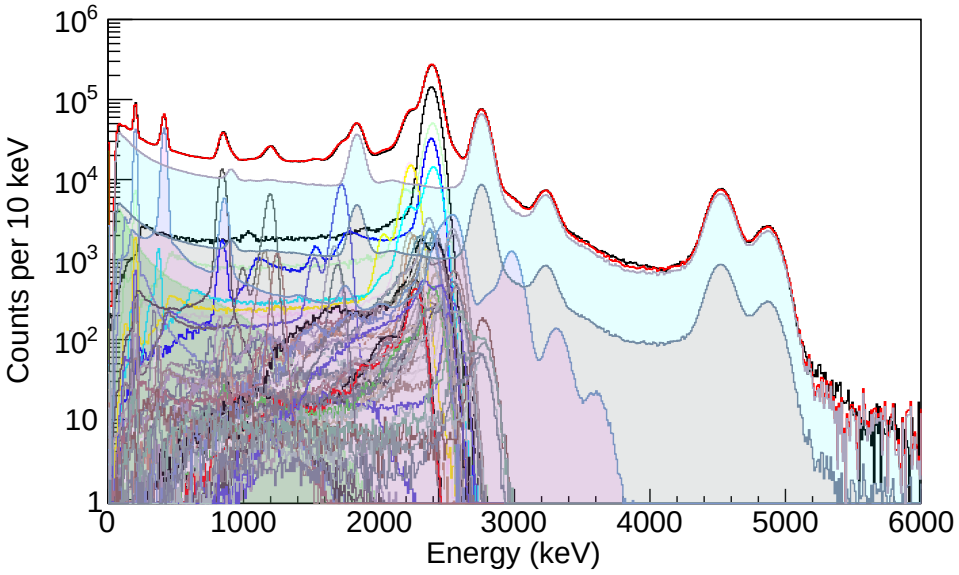

FIG. 6. Deconvolution results of the total MTAS spectrum of ^{88}Kr. Only the decay paths with feeding intensities larger than 0.1% are plotted. The blue curve is the experimental spectrum including all the neighbor nuclei contamination. The highlighted green shadow is the ground-state of ^{88}Kr. The purple shadow is the ^{87}Kr spectrum [39]. The cyan and grey shadow are the parent-related and parent-independent ^{88}Rb spectra respectively. Without fitting the time-dependent MTAS spectra (Fig. 4), the proportion of two types of ^{88}Rb spectra can not be determined.

pared the simulated beta spectrum with the measured MTAS spectrum using ^{90}Sr-^{90}Y source, which has 99.9885% ground-state feeding with $Q_\beta = 2.28$ MeV [26]. This validates the shape of the β response function.

The average MTAS β efficiency is affected not only by the correct modeling of MTAS structure, but also by the input of theoretical β spectra, which has some uncertainty for theoretical models [38, 41]. To estimate the sensitivity of the average MTAS β efficiency to the ground-state feeding, the total number of simulated ground-state feeding events is scaled independently by $\pm$10%. By doing this, the average MTAS β efficiency is scaled independently by $\pm$10%, while keeping the spectral shape of the ground-state response function unchanged. This leads to an absolute change of ground-state feeding intensity by only $\pm$2% for ^{88}Rb, and for ^{88}Kr the corresponding change is only $\pm$0.4%. As a conservative estimate, this 2% systematic uncertainty, which includes the uncertainty of the theoretical β spectra, is the largest single uncertainty for the ground-state feeding of ^{88}Rb.

2. Theoretical β shape.

It is assumed that all of the β responses are allowed transition, but this assumption is not always true. The ground-state feeding of ^{88}Rb and ^{88}Kr are both first forbidden unique transitions. By comparing the feeding intensities obtained using different ground-state response functions for allowed and first forbidden β shapes, the systematic uncertainty introduced by theoretical β spectrum is estimated. The ground-state feeding of ^{88}Rb is 78.2% if a first forbidden unique transition is applied in the deconvolution, while the number is 77.9% if an allowed transition is applied. The absolute difference caused by different β shapes is 0.3%. For ^{88}Kr, the ground-state feeding increases from 12.9% to 13.9% when an allowed transition is applied, comparing with a first forbidden unique transition.

The assumption of β shapes not only reduces the reduced χ_2 in the fit as shown in Fig. 3, but also minorly impacts the average MTAS β efficiency. For ^{88}Rb, the average MTAS β efficiency in the simulated response function is 31.9% for allowed shape, and 32.2% for the first forbidden unique shape. For ^{88}Kr, the average MTAS β efficiency in the response function is 8.6% for allowed shape, and 9.2% for the first forbidden unique shape. The average MTAS β efficiency of ^{88}Kr 9.2% is much smaller than ^{88}Rb 32.2% due to the lower Q_β of ^{88}Kr.

3. Energy calibration.

MTAS energy calibration is discussed in [26]. Energy calibration is performed not only for the MTAS spectrum, but also for the GEANT4 simulated response functions. The uncertainty introduced by the two energy calibration procedures is discussed separately.

For the MTAS experiments, all modules are gain matched PMT by PMT using the 1461 keV γ from KCl salt sources. The 1461 keV and 2614 keV γ from natural background is used for the energy calibration of each module in the data analysis.

The calibration of MTAS response functions was discussed in-depth in [31]. A linear interpolated function is applied to match 30 keV shift for the multi-γ cascades. The precision of peak center in the calibrated response functions is less than 10

keV in general compared with the peaks in the MTAS spectrum.

The impact of energy calibration to the feeding uncertainty depend on whether a level is well separated from other levels. For the well-separated levels, their feeding intensities are stable when a small shift of the peak center is considered. For ^{88}Rb, by manually changing the scale factor of energy calibration by $\pm 1\%$, the ground-state feeding changes by $\pm 0.1\%$. For the adjacent levels, their feeding intensities are anti-correlated and thus very sensitive to the calibration, but the sum of these anti-correlated feedings are stable [40]. Note that when nearby level energies are similar, this only leads to a small impact on the decay heat calculation, regardless of the anti-correlated feeding intensities of the adjacent levels.

4. Coincidence time window.

The coincidence window in the data analysis is a running time window related to the time stamp of signals from each PMT and silicon detector. Coincidence windows typically utilized in MTAS data analysis between different channels are 150 ns and 500 ns. The selection of proper coincidence window is a tradeoff between statistics and background coincidence. In this paper, 500 ns coincidence window is selected with the small cost of minorly increasing pileup and background coincidence events.

5. Pileup and background coincidence.

A pileup event is two β decay events occurring within the fast trigger time. Pileup events are rejected by the data acquisition system when there are multiple triggers in a single channel during the acquisition time, e.g. 2.7 μs, but greater than the fast trigger time of 150 ns.

A background coincidence event is an event where one decay event and one background event occurred within the coincidence window. Low event rate of MTAS (typically less than 3 kHz) is the key to minimize the pileup and background coincidence events. 6 tons of lead shielding and coincidence with beta trigger reduce the background events by three orders of magnitude. There are still a small fraction of pileup and background coincidence events in the MTAS spectra. But a simple method reproduces the pileup and background coincidence spectrum to account for them in the MTAS spectra.

Three types of pileup or background coincidence spectra are taken into account, each with its unique energy spectrum shape. 1) random coincidence of two β-decay events. This pileup spectra are obtained by convolving the total MTAS spectra with itself. 2) random coincidence of a β trigger in Si detectors and a natural background event in MTAS. This type mainly comes from part of ground-state feeding events that only provide β triggers, but deposit no energy in MTAS modules. This trigger-background spectra is exactly the same as the background MTAS spectra, which is measured during the MTAS experiments. 3) random coincidence of one β-decay event with Si and MTAS signals and one natural background event in MTAS. This source-background spectra can be obtained by convolving the total MTAS spectra with the measured background spectra. By convolving two events module by module, the Center vs. total MTAS spectra and individual module vs. total MTAS spectra only from pileup or background coincidence events are created.

Fig. 7 shows that the pileup and background coincidence spectra reproduce the MTAS spectrum of ^{88}Rb above Q_β. This is done by using the pileup and background coincidence spectra as three independent response functions to deconvolve the total MTAS spectra above Q_β. The pileup events is about one order of magnitude less than the background coincidence events. By fitting the MTAS spectrum above Q_β, the corresponding coincidence spectra reproduce the Center vs. total MTAS spectra and individual module vs. total MTAS spectra. Fig. 8 demonstrates the spectral structures above 5 MeV is well reproduced. This method allows proper accounting for pileup and background coincidence spectra, and reduces the systematic uncertainty of the feeding intensities. This also helps to rule out misinterpreted feedings to higher excited states.

6. Multiplicity of γ cascades.

The impact of multiple γ cascades on the total MTAS efficiency is discussed in [32]. The Center vs. total MTAS spectra identify the dominant decay paths and multiplicity. For weakly populated levels with higher multiplicity, this becomes more challenging. Due to the high single-gamma efficiency of MTAS [26], the ratio of 1-gamma efficiency and 4-gamma efficiency of the same total energy is $R = \varepsilon_{1\gamma}/\varepsilon_{4\gamma} \sim 1.8$ [32]. This places an upper limit on the impact of γ multiplicity on the uncertainty of total MTAS efficiency. Besides, the individual module vs. the total MTAS spectra provide additional constraints on γ multiplicity and energies [23].

Table IV, in Appendix C, lists the determined feeding intensities of individual decay paths in comparison with the corresponding feeding intensities calculated using I_β and I_γ in ENSDF data. In this table, the decay paths whose absolute feeding intensity is larger than 0.1% are identified. For the indistinguishable decay paths, the feeding uncertainties are relatively large but anti-correlated with other nearby decay paths [40]. But the summed feeding to both levels is accurate. For ^{88}Rb, the feeding to the 4846 keV level followed by 2112, 898, 1836 keV gammas and the feeding to the 4853 keV level followed by 2119, 898, 1836 keV gammas are 0.12% and 0.47% in ENSDF (sum = 0.59%), while the deconvolved intensities are 0.31% and 0.18% (sum = 0.49%). The only difference of these two decay paths is the 7 keV difference between first γ-ray, so the response functions of these two decay paths are similar and MTAS does not distinguish them. The anti-correlation of intensities for similar response functions minimizes the sensitivity of γ decay heat calculation to the multiplicity of γ cascades from higher excited levels.

The average MTAS efficiency of multiple gamma cascades can be validated by estimating the MTAS peak γ efficiency. As an example, we estimated the MTAS peak efficiency for the feeding to the 3219 keV level from ^{88}Rb decay. Based on I_γ in ENSDF and the associated single-γ MTAS efficiency [26], the average MTAS efficiency for the β-feeding to the 3219 keV level is $\varepsilon_{ENSDF} = 65.3(13)\%$. Based on feeding intensity of each decay path from the deconvolution results

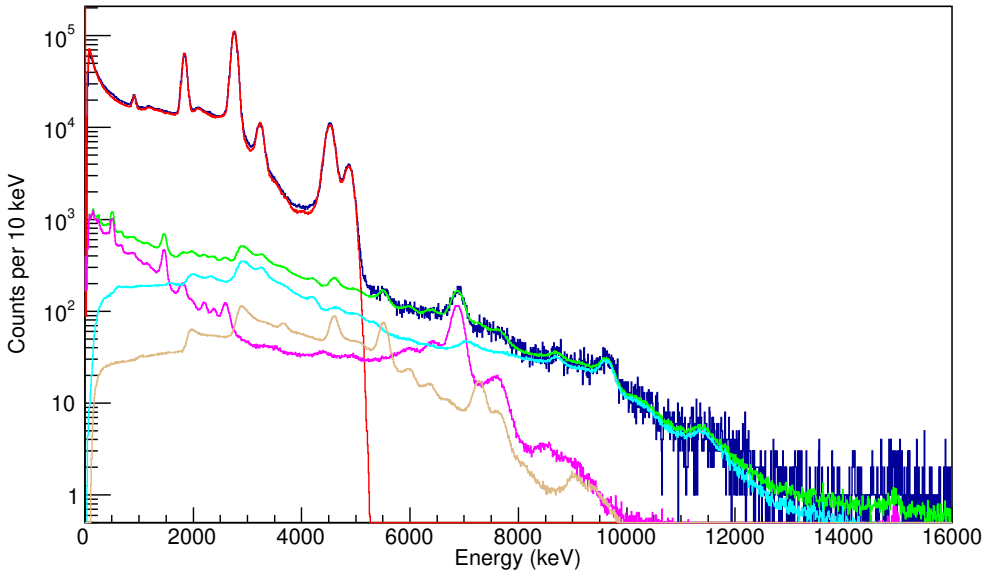

FIG. 7. This plot shows the deconvolution of total MTAS spectrum of ^{88}Rb above Q_β (5.3 MeV) using pileup and background coincidence spectra as individual response functions. The first type (brown) is the pileup spectra with two decay events, the second type (pink) is the background spectrum in coincidence with beta trigger in Si detector, the third type (cyan) is the convolution spectrum of one decay event and one background event. The blue curve is the experimental total MTAS spectrum, the red curve is the simulated MTAS spectrum. The sum spectrum of three types of background coincidence is the green curve, which reproduces the total MTAS spectrum above 6 MeV very well.

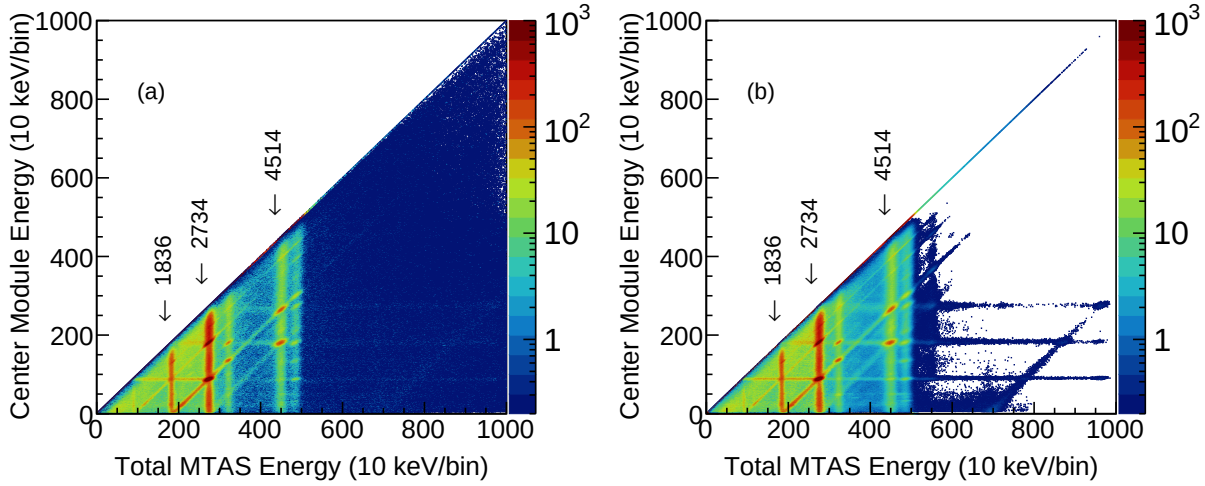

FIG. 8. (a) the two dimensional plot of Center module vs. total MTAS energy of ^{88}Rb, (b) the fitted plot including three types of background coincidence spectra.

and the simulated MTAS efficiency of each decay path, the average MTAS efficiency calculated for this level is $\varepsilon_{MTAS} = 64.6(13)\%$. These two average MTAS efficiencies obtained using alternative data sets agree well with each other.

7. Beam Contamination.

A HPGe detector is deployed near the implantation points to monitor possible beam contamination. According to the γ peaks from the HPGe spectra and the halflife of neighbor nuclei, the possible beam contamination was ^{88}Kr and ^{87}Kr.

For ^{88}Rb, there are two methods used to evaluate the impact of ^{88}Kr and ^{87}Kr contamination. First method is to use the simulated ENSDF spectrum of ^{88}Kr and ^{87}Kr decay as

TABLE III. Uncertainties introduced by different sources to the ground-state feeding of ^{88}Rb and ^{88}Kr decay. Note that these uncertainties might be correlated with others.

sources	GEANT4 simulation	β spectral shape	Energy calibration	background coincidence	Neighbor nuclei contamination	β trigger threshold	statistical
^{88}Rb	2%	0.3%	0.1%	0.3%	0.2%	0.2%	0.1%
^{88}Kr	0.5%	1.0%	0.1%	0.1%	1.0%	2.0%	0.1%

two independent response functions to fit the proportion of contamination. Second method is to subtract the MTAS spectrum in the first half (3 min) of measurement cycle with the spectrum in the second half, since the half-life of ^{88}Kr and ^{87}Kr are much longer than ^{88}Rb. The ground-state feeding intensity changes from 78.2% to 78.1% by using these two different methods, only 0.1% difference.

8. β trigger threshold.

The energy threshold of two silicon detectors is estimated to be 70 keV [26]. We investigate the impact of the beta threshold to the feeding intensities by taking into account 70 ± 10 keV in the GEANT4 simulation. The uncertainty introduced to the ground-state feeding of ^{88}Rb is only about $\pm 0.2\%$.

For ^{88}Kr, the impact of β trigger threshold is more important. The dominant feeding of ^{88}Kr is populated to 2392 keV level with β end point energy $Q_\beta - E_x = 526$ keV. The β detection efficiency of the Si detector is sensitive to the low β end-point energy [42]. By varying the β trigger threshold in the range of 60 - 100 keV in the simulated response function, $\pm 2\%$ uncertainty is introduced to the ground-state feeding of ^{88}Kr.

The estimation of the total number of decays from parent and daughter nuclei provides a hint to confirm the β trigger threshold applied in the data analysis, since the estimated total number of ^{88}Kr is sensitive with β trigger threshold while ^{88}Rb is not. The total number of decays is deduced independently from ^{88}Kr spectra, Fig. 5(a) and from parent-related ^{88}Rb spectra, Fig. 5(d). The two numbers are consistent with each other within 1σ uncertainty, which suggests the β trigger threshold of Si detector is proper.

9. Statistical error.

There are around 1.9 million counts of ^{88}Rb measured in this experiment. By analyzing the MTAS spectra obtained in different cycles, this uncertainty can be regarded as the basis of the statistical error. The data from different cycles can be analyzed independently or can be combined together. Compared with other systematic uncertainties, the statistical error is about $\pm 0.1\%$.

10. Error budget summary.

All the uncertainties that contributed to the ground-state feeding are summarized in Table III. For ^{88}Rb decay, the dominant uncertainty comes from GEANT4 simulation. For ^{88}Kr decay, the major sources of uncertain are from β threshold of the system and unseparable daughter activity.

In general, the dominant uncertainty evaluation for different β-decaying nuclei of each MTAS experiment will be different and should be reported case by case.

IV. CONCLUSIONS

This is the first reported measurement of β-feeding intensities of ^{88}Rb and ^{88}Kr using a total absorption spectrometer. The ground-state feeding of ^{88}Rb is determined to be 78.2(20)%, which is in agreement with the current ENSDF value 76.51(11)%. The ground-state feeding of ^{88}Kr is determined to be 12.9(25)%, which is also in agreement with ENSDF value 14(4)%, but the precision is improved. Validation is needed to remove doubt about specific nuclear data. The uncertainty of the β-feeding intensities for these two decays has been investigated in details. A new method to fit the cycle time vs. total MTAS energy spectra together with other MTAS spectra has been developed, allowing us to reduce the overall uncertainty in the β-feeding intensities.

Both ^{88}Rb and ^{88}Kr ground-state feeding are first forbidden unique transitions. We have applied allowed and first forbidden transition as the response function of ground-state feeding in the deconvolution procedure. In the analysis of ^{88}Rb, the reduced χ^2 is almost as twice larger when an allowed transition is applied in the simulation of ground-state feeding. This is the first case that demonstrate MTAS can distinguish the first forbidden unique transition from allowed transition by its energy spectral shape.

ACKNOWLEDGMENTS

We would like to thank the ORNL Tandem operations staff for providing the excellent quality proton beams necessary for this work. This work was partially supported through the DOE Nuclear Data program, within the FOA 18 1903 project. This research was also sponsored by the Office of Nuclear Physics, U. S. Department of Energy under contracts DE-AC05-00OR22725 (ORNL), DE-FG02-96ER40983 (UTK), DE-FG02-96ER40978 (LSU), DE-FG02-96ER41006 (MSU), DE-FG-05-88ER40407 (VU), UMO-2016/23/B/ST2/03559 from the Polish National Centre for Science. P. Shuai is supported by CSC-FRIB Postdoctoral Fellowship grant 201804910906. This work was also supported and inspired by the IAEA Coordinated Research Project for a "Reference Database for β-Delayed Neutron Emission".

* rascobc@ornl.gov

[1] J. Hardy, L. Carraz, B. Jonson, and P. Hansen, Phys. Lett. B **71**, 307 (1977).
[2] R. Greenwood, R. Helmer, M. Putnam, and K. Watts, Nucl. Instrum. Meth. A **390**, 95 (1997).
[3] R. F. M. Nitschke, P.A. Wilmarth, Lawrence Berkeley Laboratory Nuclear Science Division 1989-1990 Annual Report LBL-30798 , 111 (1991).
[4] https://www.nndc.bnl.gov/ensdf/.
[5] B. C. Rasco, M. Wolińska-Cichocka, A. Fijałkowska, K. P. Rykaczewski, M. Karny, et al., Phys. Rev. Lett. **117**, 092501 (2016).
[6] A. Fijałkowska, M. Karny, K. P. Rykaczewski, B. C. Rasco, R. Grzywacz, et al., Phys. Rev. Lett. **119**, 052503 (2017).
[7] A. Algora, D. Jordan, J. L. Taín, B. Rubio, et al., Phys. Rev. Lett. **105**, 202501 (2010).
[8] A.-A. Zakari-Issoufou, M. Fallot, A. Porta, A. Algora, J. L. Tain, et al., Phys. Rev. Lett. **115**, 102503 (2015).
[9] S. Rice, A. Algora, J. L. Tain, E. Valencia, J. Agramunt, et al., Phys. Rev. C **96**, 014320 (2017).
[10] Y. Abe et al. (Double Chooz Collaboration), J. High Energy Phys. **10**, 086.
[11] F. P. An et al. (Daya Bay Collaboration), Phys. Rev. Lett. **118**, 251801 (2017).
[12] D. Adey et al. (Daya Bay Collaboration), Phys. Rev. D **100**, 052004 (2019).
[13] J. K. Ahn et al. (RENO Collaboration), Phys. Rev. Lett. **108**, 191802 (2012).
[14] A. C. Hayes, J. L. Friar, G. T. Garvey, G. Jungman, and G. Jonkmans, Phys. Rev. Lett. **112**, 202501 (2014).
[15] A. Spyrou, S. N. Liddick, A. C. Larsen, M. Guttormsen, K. Cooper, et al., Phys. Rev. Lett. **113**, 232502 (2014).
[16] V. Guadilla, J. L. Tain, A. Algora, J. Agramunt, D. Jordan, et al., Phys. Rev. C **102**, 064304 (2020).
[17] E. McCutchan and A. Sonzogni, Nuclear Data Sheets **115**, 135 (2014).
[18] J. Lin, K. Rengan, and R. A. Meyer, Radiochem. Radioanal. Lett. **50**, 399 (1982).
[19] M. Zendel, N. Trautmann, and G. Herrmann, J. Inorg. Nucl. Chem. **42**, 1387 (1980).
[20] T. Yoshida and A. L. Nichols, Assessment of fission product decay data for decay heat calculations: A report by the working party on international evaluation co- operation of the nuclear energy agency nuclear science committee (nuclear energy agency, organization for economic co-operation and development, paris, 2007), ISBN 9789264990340.
[21] M. Gupta, M. Kellett, A. Nichols, and O. Bersillon, Decay heat calculations: Assessment of fission product decay data requirements for th/u fuel, IAEA report INDC(NDS)-0577, May 2010, IAEA, Vienna, Austria.
[22] A. A. Sonzogni, M. Nino, and E. A. McCutchan, Phys. Rev. C **98**, 014323 (2018).
[23] B. C. Rasco, K. P. Rykaczewski, A. Fijałkowska, M. Karny, M. Wolińska-Cichocka, et al., Phys. Rev. C **95**, 054328 (2017).
[24] J. R. Beene, D. W. Bardayan, A. G. Uribarri, C. J. Gross, K. L. Jones, J. F. Liang, W. Nazarewicz, D. W. Stracener, B. A. Tatum, and R. L. Varner, J. Phys. G **38**, 024002 (2011).
[25] D. Stracener, G. Alton, R. Auble, J. Beene, P. Mueller, and J. Bilheux, Nucl. Instrum. Meth. A **521**, 126 (2004).
[26] M. Karny, K. Rykaczewski, A. Fijałkowska, B. Rasco, M. Wolińska-Cichocka, R. Grzywacz, K. Goetz, D. Miller, and E. Zganjar, Nucl. Instrum. Meth. A **836**, 83 (2016).
[27] E. McCutchan and A. Sonzogni, Nucl. Data Sheets **115**, 135 (2014).
[28] R. Grzywacz, C. Gross, A. Korgul, S. Liddick, C. Mazzocchi, R. Page, and K. Rykaczewski, Nucl. Instrum. Meth. B **261**, 1103 (2007).
[29] L. B. Lucy, Astron. J. **79**, 745 (1974).
[30] J. Tain and D. Cano-Ott, Nucl. Instrum. Meth. A **571**, 728 (2007).
[31] B. Rasco, A. Fijałkowska, M. Karny, K. Rykaczewski, M. Wolińska-Cichocka, R. Grzywacz, and K. Goetz, Nucl. Instrum. Meth. A **788**, 137 (2015).
[32] B. C. Rasco, A. Fijałkowska, K. P. Rykaczewski, M. Wolińska-Cichocka, M. Karny, et al., Acta Phys. Pol. B **48** (2017).
[33] M. Stukel, B. Rasco, N. Brewer, P. Di Stefano, K. Rykaczewski, et al., Nucl. Instrum. Meth. A **1012**, 165593 (2021).
[34] R. L. Bunting, W. L. Talbert, J. R. McConnell, and R. A. Meyer, Phys. Rev. C **13**, 1577 (1976).
[35] F. K. Wohn, M. D. Glascock, W. L. Talbert, S. T. Hsue, and R. J. Hanson, Phys. Rev. C **13**, 2492 (1976).
[36] H. Miyahara, A. Yoshida, G. Wurdiyant, H. Nagata, and N. Marnada, Appl. Radiat. Isot. **56**, 163 (2002).
[37] R. Ragaini and J. Knight, Nucl. Phys. A **125**, 97 (1969).
[38] X. Mougeot, Phys. Rev. C **91**, 055504 (2015).
[39] M. Karny et al., to be published (2022).
[40] R. Greenwood, R. Helmer, M. Lee, M. Putnam, M. Oates, D. Struttmann, and K. Watts, Nucl. Instrum. Meth. A **314**, 514 (1992).
[41] L. Hayen, J. Kostensalo, N. Severijns, and J. Suhonen, Phys. Rev. C **100**, 054323 (2019).
[42] J. Agramunt, J. Tain, M. Gómez-Hornillos, A. Garcia, F. Albiol, et al., Nucl. Instrum. Meth. A **807**, 69 (2016).

Appendix A. Baysian-based iterative deconvolution algorithm

In this appendix, i, j, k and l represent the index of energy channels in MTAS spectra, and N is the total number of channels, while a and b represent the index of decay paths, and M is the total number of decay paths.

The experimental MTAS spectra d_i can be regarded as the linear combination of the MTAS response functions of each decay path R_{ia} weighted by the corresponding scale factor s_a,

$$d_i = \sum_{a=1}^{M} R_{ia} s_a, \quad a = 1, \ldots, M, \tag{2}$$

where d_i is the counts at the i-th bin in the MTAS spectrum, R_{ia} is the counts at the i-th bin in the response function of a-th decay path when simulating N_{sim} events.

The aim is to solve all the scale factors s_a from Eq. 2, so that we can calculate the feeding intensities of each decay path

$$I_a = \frac{s_a}{\sum_{a=1}^{M} s_a}, \quad a = 1, \ldots, M, \tag{3}$$

and further calculate the feeding intensities of each level I_β by adding the feeding intensities of each decay path that fed to the same level.

To solve Eq. 2, the Baysian-based iterative algorithm is a robust technique that conserves the constrains of normalization and non-negativeness of feeding probabilities. The procedure is to randomly select a set of positive non-zero $s_a^{(r=0)}$

(r is the number of iterations and $a = 1,\ldots,M$) as initial input, then use the following equations

$$s_a^{(r+1)} = \frac{1}{\sum_{k=1}^{N} R_{ka}} \sum_{i=1}^{N} \frac{R_{ia} s_a^{(r)} d_i}{\sum_{b=1}^{M} R_{ib} s_b^{(r)}}, \quad a = 1,\ldots,M. \tag{4}$$

to solve $s_a^{(r\to\infty)}$ iteratively.

Now consider a MTAS coincidence spectra d'_{ij}, the corresponding response functions are R'_{ija}. Take MTAS-center spectra as an example, i represents the energy deposit in MTAS, and j represents the energy deposit in center module. Analogy to Eq. 4, the Baysian-based iterative algorithm can be simply extended by making a transformation $d_i \to d'_{ij}$, $R_{ia} \to R'_{ija}$ and $\sum_{i=1}^{N} \to \sum_{i=1}^{N}\sum_{j=1}^{N}$. This is true because a 2-D spectrum of size $n \times n$ is mathematically equivalent to 1-D spectrum of size n^2. We get the deconvolution equation for coincidence spectra

$$s_a^{(r+1)} = \frac{1}{\sum_{k=1}^{N}\sum_{l=1}^{N} R'_{kla}} \sum_{i=1}^{N}\sum_{j=1}^{N} \frac{R'_{ija} s_a^{(r)} d'_{ij}}{\sum_{b=1}^{M} R'_{ijb} s_b^{(r)}}, \quad a = 1,\ldots,M. \tag{5}$$

Based on the fact that if $s = \frac{a}{b} = \frac{c}{d} = \cdots$ $(b, d \neq 0)$, the ratio remains the same $s = \frac{a+c+\cdots}{b+d+\cdots}$, we can fit the MTAS spectra and all kinds of coincidence spectra at the same time to constrain γ multiplicity and reduce fitting uncertainty.

$$s_a^{(r+1)} = \frac{\sum_{i=1}^{N} \frac{R_{ia} s_a^{(r)} d_i}{\sum_{b=1}^{M} R_{ib} s_b^{(r)}} + \sum_{i=1}^{N}\sum_{j=1}^{N} \frac{R'_{ija} s_a^{(r)} d'_{ij}}{\sum_{b=1}^{M} R'_{ijb} s_b^{(r)}} + \cdots}{\sum_{k=1}^{N} R_{ka} + \sum_{k=1}^{N}\sum_{l=1}^{N} R'_{kla} + \cdots}, \quad a = 1,\ldots,M. \tag{6}$$

Appendix B. Response function of MTAS energy and Bateman equation

The simulated response function of total MTAS energy for each decay path can be used to generate the two dimensional response of MTAS energy versus time, if the half-life is precisely measured. The β decay from parent nuclei follows simple exponential decay, the decay rates $A_1(t)$ follow

$$A_1(t) = \lambda_1 N_1 e^{-\lambda_1 t}, \tag{7}$$

where λ_1 are decay constant of parent nuclei, N_1 is the ion number of parent nuclei.

But the β decay from daughter nuclei are more complicated. We split the β decays from daughter nuclei as parent-related decay and parent-independent decay. For the parent-related decay, there are no decay activities at $t = 0$, the decay rates $A_2(t)$ follow,

$$A_2(t) = \lambda_2 N_1 \frac{\lambda_1}{\lambda_2 - \lambda_1}(e^{-\lambda_1 t} - e^{-\lambda_2 t}), \tag{8}$$

where λ_2 are decay constant of decay daughter. $A_2(t)$ is proportional to the ion number of parent N_1. For the patent-independent decay, the decay rates $A'_2(t)$ follow simple exponential decay.

$$A'_2(t) = \lambda_2 N_2 e^{-\lambda_2 t}, \tag{9}$$

if there are N_2 ions of decay daughter exist (implanted or grow-in) at $t = 0$. In Eq. 7-9, experimental values of λ_1 and λ_2 are known, only N_1 and N_2 are free parameters.

For the parent decay, we assume the probability to detect an event in the i-th bin (Energy) in the simulated MTAS response is R_{ia} for the a-th decay path, then the probability to detect an event at t-th bin in y-axis (Time) and i-th bin in x-axis (Energy) is

$$R_{ia}(t) = \frac{R_{ia}}{\int_0^{T_{meas}} A_1(t)dt} \int_{t-1}^{t} A_1(t)dt. \tag{10}$$

where T_{meas} is the measurement time in one MTAS measurement cycle.

For the parent-related decay, we can calculate the matrix element by just substituting R_{ia} (from parent) with R'_{ia} (from decay daughter), and substituting $A_1(t)$ with $A_2(t)$ in Eq. 10.

Appendix C. Feeding intensities of each decay path in ^{88}Rb decay

The deconvolution of MTAS spectra is based on the response functions of each decay path. Table IV lists the deconvolution results of feeding intensities for each decay path and the corresponding values calculated using β and γ intensities in ENSDF. The uncertainty of the feeding intensity of each decay path determined using MTAS only includes the fitting uncertainty.

TABLE IV. β feeding intensities of ^{88}Rb determined for each decay path in comparison of ENSDF data.

Level (keV)	γ cascade (keV)	ENSDF (%)	MTAS (%)
ground state		76.51(11)	78.2(20)
1836	1836	4.93(24)	4.22(39)
2734	2734	0.09(1)	0.36(3)
	898 - 1836	13.5(2)	12.4(11)
3219	3219	0.234(5)	0.237(22)
	1382 - 1836	0.774(15)	0.711(65)
	484 - 2734	0.0002	0.0005
	484 - 898 - 1836	0.030(7)	0.113(10)
3487	3487	0.016(11)	0.020(2)
3524	3524	0.001	0.005(1)
	1688 - 1836	0.002	0.022(2)
3635	1799 - 1836	0.0047	0.0031
	416 - 3219	0.0001	0.0002
	416 - 484 - 2734	$\sim$0	$\sim$0
	416 - 1382 - 1836	0.0003	0.0004
	416 - 484 - 898 - 1836	$\sim$0	0.035(3)
4036	4036	0.0137(21)	0.0139(13)
4224	2388 - 1836	0.030(3)	0.008(1)
4414	891 - 3524	0.007(3)	0.0001
	1680 - 2734	0.0003	0.0027
	2578 - 1836	0.186(9)	0.321(30)
	891 - 1688 - 1836	0.014(11)	0.072(7)
	1680 - 898 - 1836	0.047(6)	0.069(6)
4514	1027 - 3487	0.011(5)	0.016(2)
	1780 - 2734	0.0015	0.071(7)
	2678 - 1836	2.076(34)	1.44(13)
	1780 - 898 - 1836	0.232(6)	0.340(31)
4743	4743	0.178(19)	0.220(20)
4846	1627 - 3219	0.0021(4)	0.0043(4)
	2112 - 2734	0.0008	0.021(2)
	3010 - 1836	0.270(7)	0.225(21)
	1627 - 484 - 2734	$\sim$0	$\sim$0
	1627 - 1382 - 1836	0.007(1)	0.016(2)
	2112 - 898 - 1836	0.122(5)	0.312(29)
	1627 - 484 - 898 - 1836	0.0003	0.016(2)
4853	4853	0.012(2)	0.008(1)
	1366 - 3487	0.113(9)	0.080(7)
	2119 - 2734	0.003	0.010(1)
	3017 - 1836	0.005	0.010(1)
	339 - 1027 - 3487	0.0003	$\sim$0
	339 - 1780 - 2734	$\sim$0	$\sim$0
	339 - 2678 - 1836	0.054(3)	0.017(2)
	439 - 890 - 3524	0.0004	$\sim$0
	439 - 1680 - 2734	$\sim$0	0.0004
	439 - 2578 - 1836	0.011(3)	0.011(1)
	1218 - 416 - 3219	0.0008	0.0003
	1218 - 1799 - 1836	0.048(4)	0.033(3)
	2119 - 898 - 1836	0.469(13)	0.171(16)
	339 - 1780 - 898 - 1836	0.006	0.042(4)
	439 - 890 - 1688 - 1836	0.0008	0.0072(7)
	439 - 1680 - 898 - 1836	0.0028	0.0018
	1218 - 416 - 484 - 2734	$\sim$0	0.0027
	1218 - 416 - 1382 - 1836	0.0027	0.012(1)
	1218 - 416 - 484 - 898 - 1836	0.0001	0.046(4)

The feeding intensities for each level can be found in Table I.